

Tight junctions in the blood–brain barrier promote edema formation and infarct size in stroke – Ambivalent effects of sealing proteins

Journal of Cerebral Blood Flow & Metabolism
2021, Vol. 41(1) 132–145
© The Author(s) 2020
Article reuse guidelines:
sagepub.com/journals-permissions
DOI: 10.1177/0271678X20904687
journals.sagepub.com/home/jcbfm



Lars Winkler^{1,*} , Rosel Blasig^{1,*}, Olga Breitkreuz-Korff¹ , Philipp Berndt¹, Sophie Dithmer¹, Hans C Helms¹, Dmytro Puchkov¹, Kavi Devraj² , Mehmet Kaya³, Zhihai Qin⁴, Stefan Liebner², Hartwig Wolburg⁵, Anuska V Andjelkovic⁶, Andre Rex⁷, Ingolf E Blasig¹ and Reiner F Haseloff¹ 

Abstract

The outcome of stroke is greatly influenced by the state of the blood–brain barrier (BBB). The BBB endothelium is sealed paracellularly by tight junction (TJ) proteins, i.e., claudins (Cldns) and the redox regulator occludin. Functions of Cldn3 and occludin at the BBB are largely unknown, particularly after stroke. We address the effects of Cldn3 deficiency and stress factors on the BBB and its TJs. Cldn3 tightened the BBB for small molecules and ions, limited endothelial endocytosis, strengthened the TJ structure and controlled Cldn1 expression. After middle cerebral artery occlusion (MCAO) and 3-h reperfusion or hypoxia of isolated brain capillaries, Cldn1, Cldn3 and occludin were downregulated. In Cldn3 knockout mice (C3KO), the reduction in Cldn1 was even greater and TJ ultrastructure was impaired; 48 h after MCAO of wt mice, infarct volumes were enlarged and edema developed, but endothelial TJs were preserved. In contrast, junctional localization of Cldn5 and occludin, TJ density, swelling and infarction size were reduced in affected brain areas of C3KO. Taken together, Cldn3 and occludin protect TJs in stroke, and this keeps the BBB intact. However, functional Cldn3, Cldn3-regulated TJ proteins and occludin promote edema and infarction, which suggests that TJ modulation could improve the outcome of stroke.

Keywords

Stroke, blood–brain barrier, tight junctions, claudins, occludin

Received 4 March 2019; Revised 20 December 2019; Accepted 20 December 2019

Introduction

Brain injury with disturbed blood flow occurs in various conditions, such as trauma, inflammation or ischemia, and accounts for millions of emergencies. These include stroke – a deadly and debilitating disease which affects >15 million people worldwide each year¹ – associated in the USA with 37% mortality (2013) and 34 billion USD health costs (2014).² Ischemic stroke affects the blood–brain barrier (BBB), and this contributes to brain edema, hemorrhagic transformation, cerebral infarction, and increased morbidity. The BBB formed by endothelial cells prevents paracellular passage and uses various transport systems for supplying

¹Leibniz-Forschungsinstitut für Molekulare Pharmakologie (FMP), Berlin-Buch, Germany

²Institute of Neurology (Edinger-Institute), University Hospital, Goethe University Frankfurt am Main, Frankfurt, Germany

³School of Medicine, Department of Physiology & Koç University Research Center for Translational Medicine, Koç University, Istanbul, Turkey

⁴The First Affiliated Hospital of Zhengzhou University, Henan, China

⁵Institute of Pathology and Neuropathology, Universität of Tübingen, Tübingen, Germany

⁶Department of Pathology, University of Michigan, Ann Arbor, MI, USA

⁷Charité-Universitätsmedizin, Experimental Neurology, Berlin, Germany

*These authors contributed equally to this work.

Corresponding author:

Reiner F Haseloff, Leibniz-Forschungsinstitut für Molekulare Pharmakologie, Robert-Rössle-Str. 10, Berlin 13125, Germany.
Email: haseloff@fmp-berlin.de

nutrients or for preventing uptake of xenobiotics, thereby maintaining brain homeostasis.³ Dysfunction of the BBB is induced by oxidative/nitrosative stress, metabolic/ionic dysregulation, and inflammatory/neurodegenerative processes.⁴ BBB disruption results in extravasation and extracellular accumulation of fluid in the brain parenchyma (vasogenic edema) and elevated intracellular levels of fluid and Na⁺. This leads to cytotoxic edema which is evident as cell swelling.⁵

Tight junctions (TJs) are a key structure of a tissue barrier, and consist of multiprotein complexes regulating the passage of solutes and cells through the paracellular gap.⁶ Twenty-seven TJ proteins (26 in man) in the claudin (Cldn) family and the TJ-associated marvel proteins occludin (Occl) and tricellulin are responsible for barrier specificity.⁷ This is implemented by a tissue-specific pattern of Cldn subtypes that form intercellular TJ strands between opposing cell membranes.⁸ Depending on their function in the paracellular space, claudins are classified as tightening or channel-forming; for several claudins, an exact function has not yet been reported. Many transmembranous TJ proteins are linked to the cytoskeleton via scaffolding proteins, *Zonula occludens* (ZO) proteins play a central role in this respect.⁹

The Cldns that have been convincingly identified at the BBB are Cldn1,^{10,11} Cldn3,¹² Cldn5,¹³ Cldn11,^{14,15} Cldn12¹³ and Cldn25.¹⁵ The highest level of expression is found for Cldn5 – which is responsible for tightening the BBB for small molecules (<800 Da). In the Cldn5-deficient BBB, TJs and tightness for larger molecules are still present, suggesting that further proteins are involved.^{13,15} Compensation for Cldn3 is probably even more efficient as it is expressed at lower levels than Cldn5¹⁵ and Cldn3 knockout mice exhibit no phenotype.¹⁶ Cldn1 is weakly expressed in rodent brain microvessels.^{17,18} Patients lacking Cldn1 suffer from ichthyosis and sclerosing cholangitis,¹⁹ but without a serious phenotype at the BBB. Cldn11 localizes to the TJs and seems to have a tightening function,^{14,15} while Cldn12 does not form TJs.²⁰

Cldn3 overexpression in renal tubule cells suggests a tightening function for solutes.²¹ However, the exact role of Cldn3 at the BBB remains to be clarified.²² It has recently been shown that Cldn3 expression is greatly reduced at the blood–cerebrospinal fluid barrier (BCSFB) in patients with multiple sclerosis; other TJ proteins remained unchanged. Cldn3-deficient mice exhibit increased BCSFB permeability – in line with the earlier onset and increased severity of experimental autoimmune encephalomyelitis,¹⁶ which is a model of multiple sclerosis. A study on encephalomyelitis has found that Cldn3 is selectively lost in mouse brain capillary endothelial cells.¹² From these data, we hypothesize that Cldn3 contributes to paraendothelial

tightening at the BBB and protects TJs and, hence, the BBB endothelium from injury as during stroke.

Occl is the key marker of TJs and their redox changes; however, its impact on the ischemic and post-ischemic BBB is incompletely understood. It is highly expressed at the BBB and contributes to the barrier function, especially in vivo.²³ Occl acts as a sensor,²⁴ regulator²⁵ and protector²⁶ against redox changes, e.g., in hypoxia/ischemia or reoxygenation/reperfusion. Thus, reductants and hypoxia lower oligomerization of Occl,²⁴ its membrane localization²⁵ and interactions with Cldn1 and Cldn5.²⁷

Therefore, our aim was to elucidate the function of TJ proteins at the BBB in ischemic processes and their role in stroke. We studied molecular, cell biological and morphological alterations in Cldn3^{-/-} (C3KO)- and Cldn3^{+/+} wild type (wt) mice after transient middle cerebral artery occlusion (tMCAO) as a paradigm for stroke. These investigations were supplemented by experiments using isolated brain capillaries under hypoxic conditions. Evidence is presented that Cldn1 and Cldn3 contribute to the tightness of the BBB. Transient ischemia only slightly affects claudins and Occl, and edema clearance is retarded by the relatively intact endothelial barrier. This delay, associated with the function of the TJs, turns TJ proteins into a possible target of stroke therapy.

Material and methods

Generation of Cldn3^{-/-} mice

Cldn3-deficient mice were generated as previously described.¹⁶ Briefly, C3KO and wt mice, >8 weeks, were generated using the recombineering method²⁸ for targeted deletion of the lox-P-flanked single Cldn3 exon. Homologous recombination was performed in murine embryonic stem cells (129S7/SvEvBrd-Hprt-m2).²⁹ Correctly targeted clones identified by PCR/Southern blotting were injected into murine C57BL/6-blastocysts. Offspring of mating chimera with C57BL/6N were checked for the correct Cldn3 allele and crossed with Cre recombinase-expressing mice (C57BL/6.C-Tg(CMV-cre)1Cgn/J; Jackson Laboratory). The resulting heterozygous (Cldn3^{+/-}) animals were interbred to homozygous and wt mice, yielding an identical background. Housing of genetically modified and wt control animals and experiments were conducted according to Directive 2010/63/EU (European Parliament and Council) and the German Animal Welfare Act (as revised 4 July 2013). In accordance with guidelines and regulations, they were approved by the Animal Ethics Committee of the State Office for Health and Social Affairs, Berlin/Germany (G 0030/13) and reported by ARRIVE

(Animal Research: Reporting In Vivo Experiments). Animals were randomly allocated to different treatment groups.

Transient middle cerebral artery occlusion

The mice (male, 8–20 weeks) were anesthetized with isoflurane (Baxter, Unterschleissheim, Germany; induction 1.5–2%, maintenance 1–1.5% in 70% N₂O/30% O₂), and the left common and external carotid arteries were isolated and ligated.³⁰ A microvascular clip was placed on the internal carotid artery. For MCAO, a silicon rubber-coated monofilament (size 7–0; Doccol, Redlands, USA) was introduced through a small incision into the common carotid artery and advanced to 9 mm distal from carotid bifurcation; 30 or 60 min after the onset of the occlusion, the filament was removed under isoflurane anesthesia for complete reperfusion of the MCA for 3 h or 48 h. The internal CA was then ligated. In sham controls, the filament was removed directly after its advancement. During surgery and MCAO, body temperature was kept at 37–38°C. Typical infarction damage was caused after tMCAO. This was not the case after sham surgery as assessed by the neurological sensory-motor deficits test,³¹ the corner test³² and magnetic resonance imaging.^{33,34}

After MCAO and reperfusion, brains were frozen on dry ice and five coronal cryosections (–20°C, 20 µm) were prepared (interaaural 6.6 mm, 5.34 mm, 3.94 mm, 1.86 mm, –0.08 mm), mounted on a single Superfrost Plus glass slide, air dried, and frozen at –20°C.³⁵ The lesion was visualized by hematoxylin staining (acidic hemalum solution according to Mayer; Roth, Karlsruhe, Germany) and coverslipped with Histol 6640 and Histokit 6638 (Roth). Slides were scanned and lesion size calculated as described³¹ using ImageJ v1.49 (NIH, Bethesda, USA).

Brain capillaries: Isolation and hypoxia

Isolated brain capillaries were studied to complement the *in vivo* experiments, since certain parameters, such as the TJ ultrastructure, cannot be monitored and/or quantified in whole brain samples. These were prepared immediately after cervical dislocation, as reported.³⁶ In brief, cortices of adult mice of either sex were homogenized in Dulbecco's modified Eagle medium (DMEM with 4.5 g/l glucose; Life Technologies, Darmstadt, Germany) with a Dounce homogenizer (Wheaton, Millville, USA) on ice. An equal volume of 32% dextran (60–70 kDa, Sigma-Aldrich, Taufkirchen, Germany) was added and centrifuged (15 min, 4.500 × g, 4°C). Floating myelin was removed, the pellet resuspended in DMEM, and

filtered through a nylon mesh (41 µm; Millipore, Schwalbach, Germany). The resulting capillaries were spun down and the pellet resuspended in a small volume of DMEM. Preparations used for experiments contained >90% capillaries with <10 µm outer diameter and were divided into equal parts for all experimental groups.

Hypoxia experiments were conducted to model the effects of oxygen deprivation, the most important factor in ischemia: freshly purified capillaries were resuspended in 1.5 ml DMEM containing 20% fetal calf serum (FCS) and penicillin (100 U/ml)/streptomycin (100 mg/ml), and incubated normoxically (5% CO₂, 95% air) or hypoxically (<0.3% O₂, 5% CO₂), in an anaerobic workstation Concept Plus (Russkin Technology, Bridgend, UK, used according to the manufacturer's instructions) at 37°C for 4 h.³⁷ Hypoxic treatment did not affect cell viability.

Data on transcript expression were obtained both from isolated brain capillaries and after laser capture microdissection¹⁵ of brain slices (cf. "Additional Methods" for details).

Transendothelial electrical resistance and capacitance (Ccl) measurements of cultured endothelial cells

Mouse brain microvascular endothelial cells were isolated as described previously.³⁸ Cells were seeded in culture medium (MCDB131, 20% FCS, 100 µg/ml heparin, 5 µg/ml endothelial cell growth supplement (homemade from porcine brain), 100 U/l penicillin/streptomycin, 2 mM glutamine, 0.01 g/l NaHCO₃) on collagen I-coated wells. Endothelial cells were selected based on puromycin (4 µg/ml) resistance for two days, grown to confluency, plated at 100,000 cells/cm² onto fibronectin (Sigma-Aldrich)-coated inserts³⁹ transferred to a cellZscope instrument (nanoAnalytics, Münster, Germany), and grown for an additional five days. TER and Ccl values were obtained from continuous impedance measurements, as described.⁴⁰ Plateau values were reached after ~72 h (wt: 35.1 ± 7.4 Ω·cm²).

Immunostaining

The primary antibodies rabbit anti-human-Cldn1 (#51-9000), rabbit anti-mouse-Cldn5 (QE215213), mouse anti-human-Occl (#33-1500), mouse anti-human-ZO1 (#33-9100) and rabbit anti-mouse-Cldn3 (#34-1700) were obtained from ThermoFisher Scientific (Waltham, USA), rabbit anti-mouse-Cldn12 (JP18801) from IBL International (Hamburg, Germany) and rat anti-mouse-ZO1 (LSC124822) from Biozol Diagnostica (Eching, Germany). The secondary antibodies Alexa-Fluor 555 goat anti-rat

(#A-21434), Alexa-Fluor 488 goat anti-rabbit (#A11029), Alexa-Fluor 488 goat anti-mouse (#A32723), Alexa-Fluor 647 goat anti-mouse (#A21236) and goat anti-mouse Cy3 (#A10521) were from ThermoFisher Scientific. Hoechst 33342 (Life Technologies) was used for nuclear staining (5 μ M).

Isolated capillaries were fixed and permeabilized with 4% paraformaldehyde/0.2% Triton X-100 (Sigma-Aldrich) in phosphate-buffered saline (PBS), followed by blocking for 30 min with 0.1% Tween-20 and 2% bovine serum albumin (BSA) in PBS. Samples were incubated overnight at 4°C with primary antibodies, spun down and incubated for 30 min at RT with secondary antibodies. Samples were washed once in PBS containing 0.1% Tween-20 and 2% BSA, once in PBS, and then suspended in PBS and added to a coverslip for confocal laser scanning microscopy (LSM 510 FCS, using an Axiovert 135 microscope equipped with a Plan-Neofluar 64 \times /1.3 or 100 \times /1.3 objective; Zeiss, Jena, Germany). Background fluorescence and unspecific binding of secondary antibodies were tested in the absence of primary antibodies.

After sacrificing the mice, brains were removed and immediately frozen in 2-methylbutane on dry ice for 10 min. Brains were embedded in Tissue-Tek (AMS Biotechnology, Abingdon, UK) and 20 μ m sections were sliced using a cryostat (Cryostat CM 3000; Leica, Wetzlar, Germany). The sections were mounted on glass slides and fixed in -20°C methanol for 10 min and rehydrated with PBS. Tissue sections were blocked (2% BSA, 0.05% Triton X-100 in PBS) for 45 min at RT and incubated with the primary antibodies in PBS, supplemented with 0.1% BSA at 4°C overnight. After washing four times with PBS, the samples were incubated with the secondary antibodies at RT for 1 h and enclosed in Roti-mount FluorCare DAPI (Roth). Microscopy was performed using a Zeiss LSM 780 with an EC plan Neofluar 40 \times /1.3 or Plan apo 63 \times /1.4 oil objective and ZEN image browser software (Zeiss). For image analysis, fluorescence intensities were quantified and the Pearson colocalization coefficient was calculated via ImageJ (NIH, Bethesda, USA).

Electron microscopy

For transmission electron microscopy (TEM) following tMCAO, mice were transcidentally perfused with 4% paraformaldehyde in PBS and brains were postfixed in 2.5% glutaraldehyde for 24 h. After washing, tissue was sliced on a vibratome, osmificated in 1% OsO₄ (cacodylate buffer) for 1 h, contrasted en bloc by 1% uranyl acetate, and dehydrated in graded methanol followed by propylene oxide-assisted infiltration of epoxy resin. After a third change into pure epon, brain slices

were flat embedded and polymerized. Slices from control and tMCAO brain areas were identified and sectioned at ultramicrotome. Following 1% uranyl acetate and lead citrate contrasting, ultrathin sections were viewed in a Zeiss 900 TEM at 80 kV.

For freeze-fracture electron microscopy, capillaries were isolated and fixed with 2.5% glutaraldehyde in PBS with Ca²⁺/Mg²⁺ (PBS^{+/+}) for 2 h at RT. Capillaries were then washed twice with PBS^{+/+} to be processed for freeze-fracturing as described.⁴¹

In vivo permeability assays

Mice (10–19 weeks, either sex) received 5 μ l/(g body weight) 4% Na-fluorescein (Sigma-Aldrich) or 1% Evans blue (Sigma-Aldrich) in PBS i.v. Mice were treated 10 min after tracer injection with ketamine (0.18 mg/g; CP-Pharma, Burgdorf, Germany)/xylazine (0.024 mg/g; Ceva Tiergesundheit, Düsseldorf, Germany) and then perfused with 25 ml PBS^{+/+} and 250 U/ml heparin (Ratiopharm, Ulm, Germany) transcidentally (2 ml/min). Brains and livers were homogenized in a Dounce homogenizer in PBS^{+/+}. The fluorescent dyes were extracted by trichloroacetic acid (30% final; Roth) overnight at 4°C in the dark and centrifuged at 19,000 \times g (15 min, 4°C). The fluorescence of the supernatant was determined using a fluorescent plate reader (Tecan safire, Tecan, Maennedorf, Switzerland): Evans blue, λ_{exc} 620 nm/ λ_{em} 680 nm; fluorescein, λ_{exc} 485 nm/ λ_{em} 520 nm. Uptake of the dyes was quantified via a standard curve and calculated as μ g_{dye}/mg_{brain}.

Horseshoe peroxidase (HRP type II, Sigma, St. Louis, USA; 200 mg/kg in 100 μ l saline, i.v.) was injected into male adult mice under anesthesia (100 mg/kg choral hydrate, 35 mg/kg Na-pentothal; i. p.) to assess BBB permeability by ultrastructure; 30 min later, animals were perfused transcidentally with 25 ml saline followed by 100 ml fixative containing 2.5% glutaraldehyde and 2% paraformaldehyde in 100 mM phosphate buffer (pH 7.4) for 15 min, and kept at 4°C overnight; 50 μ m coronal sections were incubated in 0.05% 3,3'-diaminobenzidine in 50 mM Tris-HCl buffer (pH 7.6) containing 0.01% H₂O₂ for 30 min to visualize HRP-reaction products. For ultrastructural observations, samples were post-fixed in 1% OsO₄ for 1 h, dehydrated in ethanol and embedded in Epon; 60 nm sections were then examined using a JEOL 1011 (Tokyo, Japan) TEM equipped with a CCD camera (MegaView III, Soft Imaging System, Germany).⁴²

To analyze leakage of endogenous mouse IgG, mice were anesthetized with ketamine/xylazine and perfused with PBS^{+/+} and heparin as described above. Staining for β -catenin (Ctnnb1, BD Transduction), and mouse

immunoglobulin G were performed on 10 μm cryosections. Glass slides with cryosections were defrosted on a heating plate at 40°C for 10 min, followed by washing with PBS. Cryosections were then incubated in permeabilization buffer (1% BSA, 0.5% Triton X-100 in PBS) at RT for 1 h. Sections were incubated with primary antibodies, diluted in antibody incubation buffer at 4°C overnight. After washing with PBS, cryosections were incubated for 1 h with corresponding secondary antibodies, conjugated with Alexa Fluor 488 or 568, diluted in antibody incubation buffer (0.5% BSA, 0.25% Triton X-100 in PBS pH 7.2). The permeability of brain vessels on sections was tested by using a donkey anti-mouse Alexa Fluor 488 conjugated antibody (for mouse IgG staining). Sections were washed with PBS and then incubated for 10 min with 300 μM TO-PRO-3 (ThermoFisher Scientific, Darmstadt, Germany), diluted 1:10,000 in PBS for nuclear staining. After washing with PBS, sections were mounted in Aqua-Poly/Mount (Polysciences Europe, Germany).

Statistics

Data represent mean \pm SD, obtained by the two-tailed Mann–Whitney test, which was chosen when normal distribution was not demonstrable; differences were considered significant if $p < 0.05$, $n \geq 4$. For mouse experiments, differences were considered significant if $p < 0.05$, $n \geq 6$.

Results

Claudin-3 is involved in tightening the blood–brain barrier

Cldn3 knockout (C3KO) mice were compared to wt mice with regard to the contribution of Cldn3 to BBB permeability. Immunofluorescence staining of endogenous mouse immunoglobulin G (IgG, 150 kDa) pointed to augmented extravasation of endogenous proteins from some cortical capillaries of C3KO mice, whereas in vessels of wt cortices, no substantial IgG leakage was detectable (Figure 1(a)). Cerebral water content was comparable between the groups: C3KO, $76.23 \pm 0.69\%$; wt, $76.20 \pm 0.52\%$.

Horseshoe peroxidase uptake (i.v. administration; HRP, 44 kDa) was not observed in wt brains, while widespread HRP uptake was observed macroscopically in cortical and subcortical regions of C3KO mice (frontoparietal cortex, hippocampus, thalamic nuclei, striatum; Figure 1(b) left). TEM showed that endothelial cells of wt capillaries were largely free of HRP vesicles; TJs between the cells appeared ultrastructurally intact and no sign of paracellular HRP was observed 12 h after administration (Figure 1(b) right, upper

micrograph). In C3KO mice, the cytoplasm of capillary endothelial cells in the cerebral cortex, hippocampus and thalamus frequently exhibited HRP-containing vesicles located close to luminal or abluminal plasma membranes (Figure 1(b) right, lower micrograph). In C3KO brains, endothelial cells of venules and arterioles were also rich in HRP-positive vesicles. HRP was not observed outside the endothelium, either in interendothelial clefts, or in subendothelial space, basement membrane, pericytes, or in the neuropil (Figure 1(b) right, middle micrograph). The TJs appeared normal (asterisks; Figure 1(b) right).

After i.v. injection of fluorescein (376 Da), cerebral intake was doubled in C3KO (60 ± 3 ng/mg) compared to wt mice (29 ± 1 ng/mg) (Figure 1(c)). Brain uptake of Evans blue – which is known to bind to the albumin (66 kDa) fraction – tended to be increased in Cldn3-deficient mice (by approx. 38%). BBB permeabilization for small molecules was confirmed by reduced trans-endothelial electrical resistance (TER) and by an increase in the capacitance (Ccl) of a barrier formed by capillary endothelial cells isolated from C3KO brains, in comparison to those from wt animals (Figure 1(d)). Taken together, deficiency in Cldn3 leads to increased paracellular permeability of ions and small molecules, accompanied by higher endocytosis of proteins by the endothelium.

Claudin-3 maintains claudin-1 expression and tight junction complexity in the blood–brain barrier

To clarify whether the elevated BBB permeability in Cldn3-deficient mice (Figure 1) was caused by alterations in TJ proteins, we studied expression and localization patterns of these proteins in isolated brain capillaries. In wt capillaries, mRNA levels of Cldn3 and Cldn1 were relatively low compared to other junctional proteins, such as Cldn5, Occl, and ZO-1 (Figure 2(a)); Cldn1 and -3 colocalized with the junction marker ZO-1, as Cldn5 and Occl did (Figure 2(b), arrows). In addition, Cldn1 and -3 could also be detected outside the junctions (Figure 2(b)). In C3KO capillaries, Cldn1 mRNA was downregulated by about 50% (Figure 2(a)), and the protein was found preferentially outside the junctions in endothelial cells. Cldn5 and Occl maintained colocalization with ZO-1 in C3KO capillaries (Figure 2(b)). The expression of endothelial markers – such as glucose transporter 1 (Glut1) (Figure 2(a)) and vascular endothelial cadherin – remained unchanged.

Freeze-fracture electron microscopic analysis revealed numerous (30–40 meshes/ μm^2) small (diameter, 100–300 nm) meshes in the TJ network where the particle strands were equally associated with the E- and P-faces (48% and 52%) in the wt (Figure 2(c))

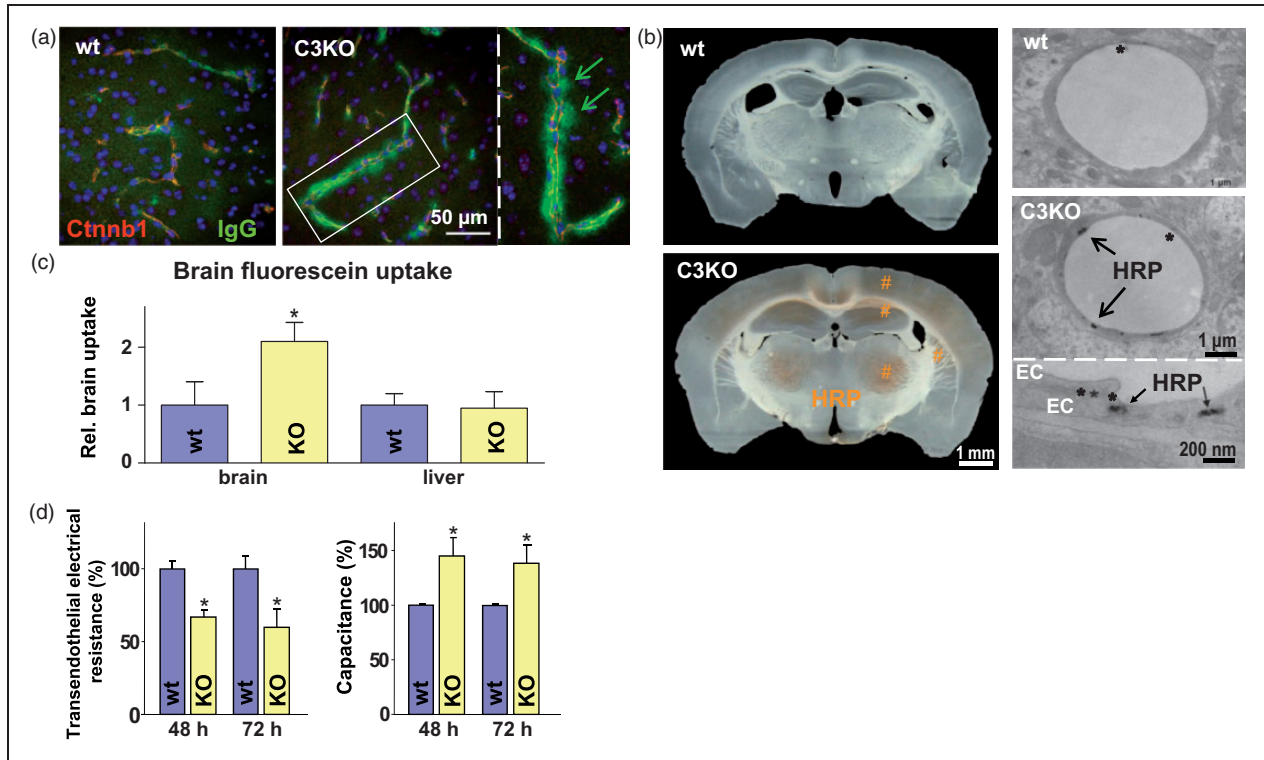


Figure 1. Claudin-3 knockout (C3KO, KO) moderately permeabilizes the blood–brain barrier (BBB) as it promotes cerebral uptake of small molecules and proteins, compared to the wild type (wt) control. (a) Immunohistochemistry shows extravasation of endogenous immunoglobulin G (IgG, arrows) from mouse brain capillaries visualized by β -catenin (Ctnnb1); blue, TO-PRO3. (b) Uptake of horseradish peroxidase (HRP, #) into the C3KO brain (macrographs, left). Transmission electron microscopy demonstrates HRP in claudin-3-deficient endothelial cells (EC) forming tight junctions (*; micrographs, right panel). (c) Increased cerebral Na-fluorescein, mean \pm SD, $n \geq 6$; *, $p < 0.05$ vs. wt brain; unpaired t -test, one-tailed. (d) Reduced transendothelial electrical resistance (left) and increase in the respective capacitance – reflecting paracellular permeability (right) of monolayers from primary brain capillary EC cultures of KO mice compared to wt at time points corresponding to confluent monolayer post seeding; mean \pm SD, $n = 4$; *, $p < 0.05$ vs. the respective wt; t -test.

left). Cldn3 deficiency resulted in fewer (~ 20 meshes/ μm^2) but larger and more elongated meshes (up to 700 nm), as a result of fewer branch points. In addition, the Cldn3-deficient TJ network exhibited slightly more E-face association in the majority of replicas (61%) and a lower density of particles on the strands (Figure 2(c) right). Quantification of the mean mesh area of the TJ network of the E-face association gave $0.022 \pm 0.002 \mu\text{m}^2$ for the wt and $0.069 \pm 0.025 \mu\text{m}^2$ for the C3KO group (Figure 2(d)), thus confirming that Cldn5 forms meshes with larger diameters than Cldn3.⁴³ The alterations were accompanied by 50% reduction in the number of branching points within the network (Figure 2(c) triangles); Figure S3 describes how these effects could influence paracellular diffusion. Thus, deficiency in Cldn3 downregulated Cldn1 transcript and redistributed the protein to the cytosol, and led to less complex TJ strands and fewer TJ meshes – corresponding to loosening of the TJ strand network.

Acute ischemia in mice: Claudin-1, -3 and occludin preserve tight junctions of the blood–brain barrier but contribute to cerebral injury

As we observed increased BBB permeability in the C3KO group, the question arose whether loss of Cldn3 influences the TJs under pathological conditions affecting the BBB.⁴⁴ For this reason, we studied the effect of ischemia on the TJs of the brain microvasculature after 60 min tMCAO and 3 h reperfusion (short-term injury). For analysis of TJ protein expression, the respective capillaries were excised by laser capture microdissection. In wt capillaries, Cldn3 mRNA expression decreased by about 73% in the postischemic area compared to the respective contralateral region (corresponding decrease for: Cldn1, 14%; Cldn12, 35%; Occl, 18%). In contrast, the level of Cldn5 mRNA increased by about 60%. In the C3KO group, the decline in Cldn1 after acute ischemia was even more remarkable (by 84%). The presence of a lesion was

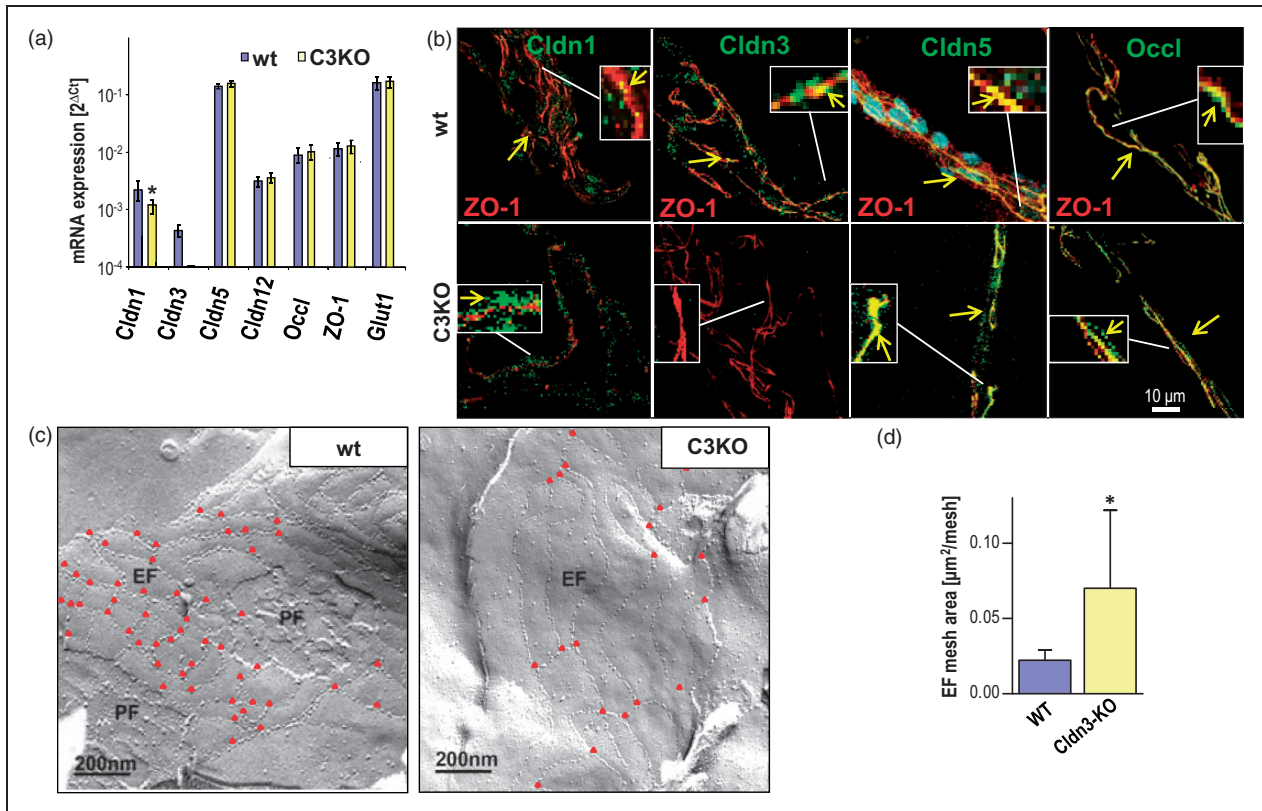


Figure 2. Isolated brain capillaries of claudin-3 knockout (C3KO) mice exhibit less complex tight junctions (TJs) and changes in expression and localization of TJ proteins, compared to the wild type (wt) control. (a) mRNA of junction proteins of C3KO, normalized to β -actin mRNA, was unaffected except that of claudin-1 (Cldn1), which was reduced. Mean \pm SD, $n = 6$; * $p < 0.05$ vs. wt; Mann–Whitney test. Glucose transporter (Glut)-1 was used as endothelial marker. (b) Immunocytochemistry revealed that Cldn1, Cldn3, Cldn5 and Occl colocalized with Zonula occludens protein 1 (ZO-1, served as a cell contact marker) in wt, which was also observed for Cldn5 and Occl in C3KO (arrows). In wt, Cldn1 and -3 appeared in the cytosol. In C3KO, Cldn1 was redistributed from the junctions to the cytosol. (c) Freeze-fracture electron microscopy revealed a less complex TJ strand network in C3KO, visualized by fewer branching points (red triangles), larger and fewer meshes, and reduced degree of P-face associated strands. EF, PF – exoplasmic, protoplasmic face association of intermembranous TJ strands. (d) TJ strand mesh size in the EF was enlarged in C3KO compared to wt. Mean \pm SD; $n = 9$, Mann–Whitney test; *, $p \leq 0.05$.

confirmed by upregulation of the ischemia marker heparin-binding epidermal growth factor-like growth factor,⁴⁵ of which the expression was more than doubled (Figure 3(a)).

In parallel to the lowered expression of Occl mRNA (Figure 3(a)), the length of Occl-positive cell contacts was reduced in the lesion areas (Figure 3(b)) of C3KO (loss, $43.3 \pm 28.2\%$) and wt groups (loss, $29.1 \pm 40.3\%$; Figure 3(b) right columns). Similarly, the length of cell contacts with Cldn5 immunoreactivity tended to be shortened in the lesion region – by $20.1 \pm 38.3\%$ in wt brains and by $25.5 \pm 38.2\%$ in those of C3KO ($n = 49$ – 61). These results confirm a decreased level of the TJ regulator Occl and suggest loss of tightening molecules of Cldn5, which was more pronounced in the affected postischemic C3KO brain endothelium.

Three hours after tMCAO, significantly shorter TJs in C3KO were visualized by TEM (examples given in

Figure 3(c), Fig. S1 upper panel). The TJ length – electron-dense material between endothelial plasma membranes – was reduced by 46% (wt, reduction by 24%). In addition, 100% of C3KO endothelium showed blebbing into the vessel lumen (wt only 30%). Similarly, 90% of C3KO endothelial cells exhibited swelling, compared to 10% of wt endothelial cells (Figure 3(d) upper part, Fig. S1 upper panel). This suggests greater endothelial injury after ischemia in the C3KO than in the wt group, possibly caused by partial loss of hydration control due to an impact of the defective TJ structure on the cell polarity. In contrast, the surrounding astrocytic endfeet were evidently more swollen in the wt control than in the C3KO group. Consequently, 12% of the endothelial surface in C3KO was exposed to swollen astrocytic endfeet, whereas 56% of the wt endothelium was adjoining to swollen perivascular structures (Figure 3(d) lower part,

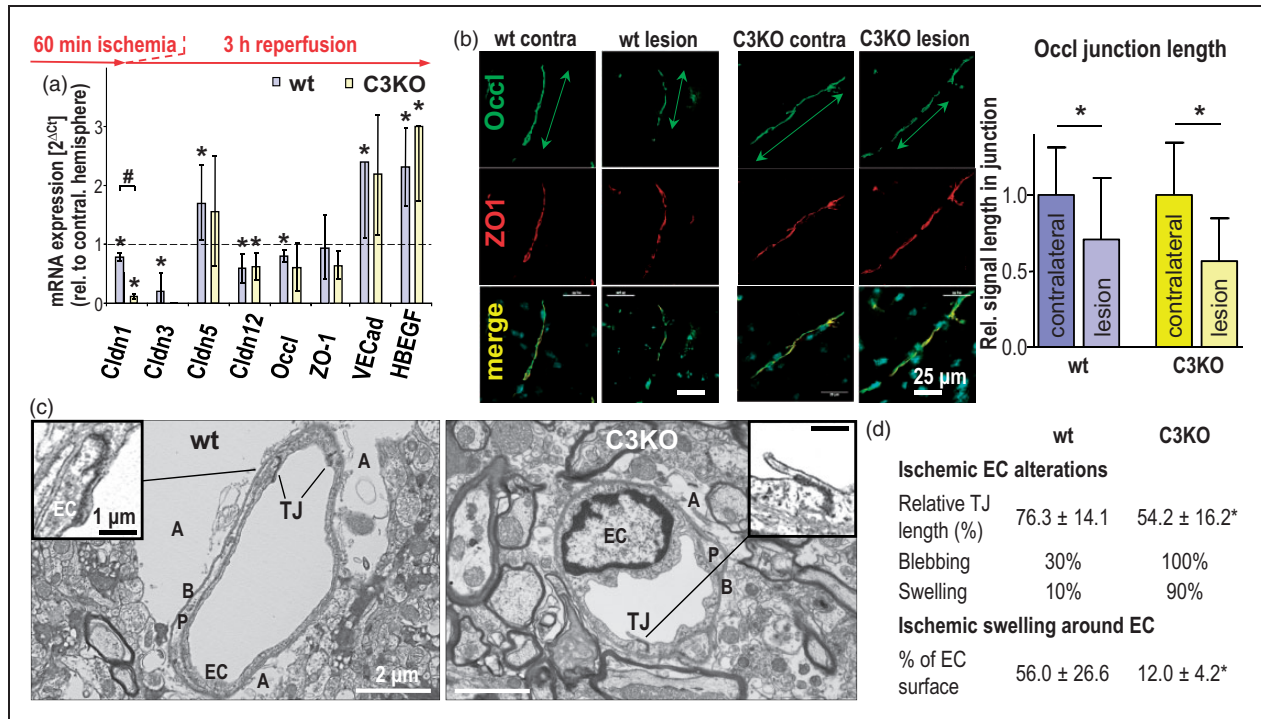


Figure 3. Acute ischemic injury (60 min middle cerebral artery occlusion followed by 3 h reperfusion) alters the expression of tight junction (TJ) proteins and their junctional localization in cerebral capillary endothelial cells (EC), resulting in more EC damage but less perivascular lesions in claudin-3 knockout (C3KO) than in wild type (wt) mice. (a) mRNA normalized to 28S ribosomal RNA (28SRNA) in postischemic brain capillaries excised by laser capture microdissection. Mean \pm SD, $n = 4$; * $p < 0.05$ compared to the respective value in the contralateral hemisphere (dashed line) and $^{\#}p < 0.05$ vs. wt, using Mann–Whitney test. Cldn: claudin; Occl: occludin; ZO-1: Zonula occludens protein 1; VECad: vascular endothelial cadherin; HBEGF: heparin-binding epidermal growth factor-like growth factor (used as an indicator of ischemic injury⁴⁵). (b) Immunohistochemistry of Occl showed decreased localization in cell contacts (reduced length of Occl-positive junctions measured along the vascular axis); ZO-1 served as cell contact marker. Mean \pm SD, $n = 41$ –61; * $p < 0.05$. (c) Transmission electron microscopy of the postischemic neurovascular unit exhibited reduced TJ length, stronger EC swelling and less swollen astrocytic endfeet in the lesional region of the C3KO brain compared to the respective wt brain; A: astrocytic endfeet; B: basement membrane; P: pericyte. (d) Quantification of the ultrastructural alterations in the vascular part of the neurovascular unit due to acute ischemic injury. The swelling around capillary endothelial cells was determined as the proportion of swollen astrocyte endfeet surrounding the abluminal part of the capillaries in electron microscopic images. Mean \pm SD, $n \geq 10$; * $p < 0.05$.

Figure S1 upper panel). Taken together, the absence of Cldn3 appeared to intensify the depletion of TJ proteins – including Cldn1 and junctional Occl – and augmented endothelial injury in the early postischemic phase. Unexpectedly, TJ damage and endothelial defects upon Cldn3 deficiency were accompanied by less swollen astrocyte endfeet after ischemia than in the wt.

Acute hypoxia of isolated brain capillaries: Claudin-3 preserves junctional occludin and tight junction structure

Isolated brain capillaries were analysed after 4 h of hypoxia, the main pathogenetic factor of ischemia, for a more detailed investigation of the observed influence of Cldn3 on acute ischemic alterations after tMCAO as shown in Figure 3. In hypoxic capillaries from

C3KO mice, the shape of the TJ marker Occl in cell contacts was less intense and more fragmented than in capillaries from wt; this was visualized by costaining with the junction marker ZO-1 (Figure 4(a)). Similarly, reduced immunoreactivity of Occl has already been reported in rat brain microvessels after 1 h of hypoxia.⁴⁶ As with Occl, Cldn5 staining at the junction was less intense in the C3KO group (additional experiments).

Hypoxia-induced changes in the immunoreactivity in capillary preparations were paralleled by diminution of the mRNA expression of Cldn1 and Cldn3. The transcript of Glut1 was upregulated under hypoxia, indicating typical hypoxia-induced disturbances (Figure 4(b)).

Hypoxic alterations in localization and expression of TJ proteins were mirrored by considerable alterations in the shape of the TJ strand network, as depicted by freeze-fracture electron micrographs. Under normoxic

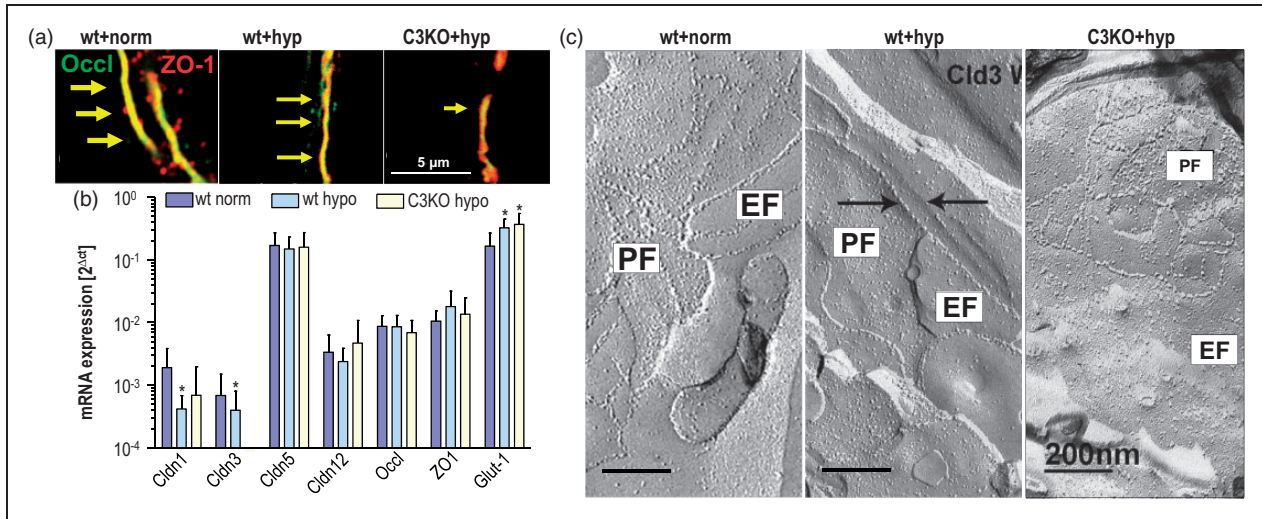


Figure 4. Four hours of hypoxia (hyp) reduces junctional localization of occludin (Occl) in isolated brain capillaries from wild type (wt) and claudin-3 (Cldn3) knockout (C3KO) mice as well as P-face association of the tight junction (TJ) strand network in C3KO. (a) In immunocytochemistry, Occl was diminished in wt hypoxia and to a greater extent in C3KO hypoxia, compared to the normoxic wt control; Zonula occludens protein 1 (ZO-1) served as junction marker; arrows indicate reduced fluorescence intensity and junctional localization of Occl. (b) The mRNA expression of Cldn1 and -3, normalized to β -actin mRNA, decreased after hypoxia compared to the normoxic wt control. Glucose transporter (Glut)-1 served as (upregulated) hypoxia marker; mean \pm SD, $n > 4$; *, $p < 0.05$ vs. wt+norm. (c) Reduction in TJ strand network by hypoxia both in wt and C3KO, and, in addition, preferential reduction in protoplasmic fracture face (PF)-associated TJ strands in the C3KO group compared to that of the wt control, visualized by freeze-fracture electron microscopy (representative images, $n = 5-25$). Note that the particle number in the strands was reduced in wt (right arrow, particle free ridge), even though the PF/EF ratio was increased. In the hypoxic C3KO group, the TJ area was generally smaller, and the EF association predominated PF association. EF: extracellular fracture face-associated TJ strands.

conditions, the TJ strand network exhibited comparable P- and E-face association (52% PF, 48% EF). In wt hypoxia, the relative P-face association was greater (69% PF, 31% EF), but the mesh size was enlarged and the number of particles on the strands decreased. In hypoxic C3KO, the strand network was even less developed. Relative to wt normoxia, P-face association greatly decreased (20% PF, 80% EF), since the contribution of Cldn3, a P-face-associated TJ protein,²⁰ is absent (Figure 4(c)). Overall, Figure 4 indicates that Cldn3 may lessen hypoxic loss of Occl from the junctions and may prevent profound degeneration of the TJ network. The decreased levels of Occl and Cldn5 found after acute hypoxia of Cldn3-deficient capillaries are comparable with the alterations early after ischemia (Figure 3). It is conceivable that the degeneration of the TJ strand network observed in hypoxic capillaries in vitro is similar to the effects occurring at the TJs of the capillary system in situ after occlusion.

Claudin-3 increases ischemia-induced injury and exacerbates swelling in mice brain by maintaining tight junctions and occludin at the blood-brain barrier

We studied the extent of cerebral damage in relation to TJ disruption and TJ protein disorder 48 h after 30 min

of transient left MCAO, in order to investigate the long-term impact of Cldn3 deficiency on ischemic stroke. Compared to wt, C3KO brains show both a smaller infarct volume (box plot) and less edema formation (column diagrams) in the affected ipsilateral side (Figure 5(a)). As indicated by TEM, the edema was obviously due to astrocytic swelling and appeared to be more intense in the wt group; in particular, electron micrographs revealed swollen astrocyte processes (Figure 5(b), Figure S1 lower panel). Moreover, multiple residues of dead cells were found in the striatal neuropil from the stroke site of wt animals. Coherence between dendrites, their processes and axons, was disturbed with increased extracellular space. Spines, dendritic shafts and axonal terminals contained vacuolar structures. The number of synaptic vesicles was decreased in swollen axonal terminals, and the remaining synaptic connections indicated signs of excitotoxicity and degradation. In C3KO mice, the injury, at least in the perivascular space, was less intense. In capillaries of wt infarcts, electron dense TJs were identified between surface membrane segments of endothelial cells in 90% of the images; $67.3 \pm 4.7\%$ of the length of these cell membrane contacts were electron dense; 2/3 of the electron dense material appeared of normal dark black color and 1/3 of this material was brightened (Figure 5(b) left).

Identification of TJs in cell surface contacts of C3KO capillaries was possible in only 43% of the images. In these, $48.8 \pm 4.6\%$ of the junction length contained electron dense material, 1/3 normal and 2/3 brightened (Figure 5(b) right).

The ultrastructural TJ injury was accompanied by a decrease in Occl levels in cell–cell contacts, as shown by immunohistochemistry (Figure 5(c) top). The length of Occl-positive fluorescent segments at the junctions was reduced in the infarction area; this injury was more developed in the C3KO group than in the wt group (64% vs. 46%, Figure 5(c) bottom, column diagram). Cldn5-positive junction segments, identified using ZO-1 as a junction marker and normalized to the contralateral area, were also shortened in infarcted brains in both groups.

In contrast to the alterations in protein distribution in the infarcted junctions, mRNA expression did not change much. Occl levels corresponded to the control values of the contralateral region in both groups. Only the transcript of Cldn1 in the C3KO infarction area remained strikingly downregulated compared to the contralateral hemisphere, and Cldn5 mRNA tended to be enhanced in both wt and C3KO infarct zones (Figure S2). Morphological observations and expression data suggest that Cldn3 is involved in the proper assembly, at least of Occl, and possibly also of Cldn5, in the TJs of the infarcted BBB. This includes adequate Cldn1 expression and promotes BBB function by maintaining the TJs, but, on the other hand, exacerbates the swelling and size of the affected site.

Discussion

This study investigates how TJ proteins determine the structure and function of the neurovascular unit, predominantly its vascular part, under normal and pathological conditions. It is found that Cldn3 contributes to the expression and localisation of other TJ proteins, to the structure and morphology of the TJs as well as to the tightness of the BBB. After ischemic disturbances, intact TJs are accompanied by periendothelial swelling of astrocytic endfeet; Cld3 deficiency is paralleled by endothelial injury, but with reduction in edema formation and infarct size.

The TJs of the BBB are believed to be mainly formed by Cldn5 under the control of Occl.⁸ Both TJ tightness and expression of TJ proteins are diminished after stroke.⁴⁷ Nevertheless, knockout of Occl has no direct impact on barrier function⁴⁸; Cldn5 deficiency causes BBB leakage only for small molecules, and TJs exhibit normal electron density in TEM.¹³ These reports suggest that further TJ proteins contribute to paracellular barrier function at the BBB. Cldn1 and Cldn3 are well recognized tightening proteins expressed

at the BBB,⁸ which we found to be downregulated after ischemic and hypoxic events. Both Cldns mediate paracellular tightening in other cell barriers^{12,17}; they associate with and influence Cldn5²⁰ as well as Occl.²⁷ Accordingly, Cldn1 and -3 are postulated to be involved in TJ formation at the BBB (despite contradictory recent results⁴⁹). In our study, Cldn1 is detected in the TJs of the barrier-forming endothelium, but also intracellularly. Thus, the contribution of Cldn1 to strengthening the tightening function at the BBB should be less important than that of Cldn3. Moreover, in the absence of Cldn3, Cldn1 is redistributed from the membrane to the cytosol, which prevents any direct function in cell contacts.

Downregulation and redistribution of Cldn1 most likely contribute to the leak in the BBB for small molecules and ions in Cldn3-deficient mice. A similar effect has been demonstrated for the Cldn1-deficient epidermis where 600 Da tracers pass through the TJs. In this context, it is interesting that Cldn1 elimination causes lethal water loss and poorly developed TJs in the epidermis.¹⁷ Paracellular fluid movement is also increased in the liver after exclusion of Cldn3.⁵⁰ Similarly, at the Cldn3-deficient BBB, we observe the passage of a 376 Da tracer and of ions, less tissue swelling and less complex TJ strands. We therefore expect water leakage through Cldn1- and Cldn3-free TJs. The transferability of tightening properties of Cldn3 from epithelial to endothelial barriers is indirectly confirmed by another study, in which Cldn3 overexpression in kidney cells reduces paraepithelial permeability.²¹ Moreover, our results correspond to an earlier study where loss of Cldn3 impairs the sealing of the epithelium in the BCSFB for solutes¹⁶ – which further supports the view that Cldn3 enhances tightening in general.

The main alterations in Cldn3-deficient mice are in the frontoparietal cortex, hippocampus, thalamic nuclei and striatum. This suggests preferred expression of Cldn3 or reduced compensation by other TJ proteins in these areas, and, possibly, heterogeneity of blood flow disturbances. On the other hand, the BBB in most cerebral capillaries appears to be tight,⁵¹ and there were no evident differences in the cellular and molecular composition of the neurovascular unit in human white and gray matter.⁵² Microvessels were more permeable, containing fenestrations, discontinuous TJs⁵³ and less TJ-associated proteins^{54,55} only at the level of circumventricular organs, especially in their central regions.

In Cldn3-deficient brains, enhanced uptake of small molecules and of protein points to increased permeation through the BBB. The loss of Cldn3 in primary brain endothelial cells causes alterations in electrical resistance and capacitance which reflect greater paracellular ion permeability.⁴⁰ Bearing in mind the

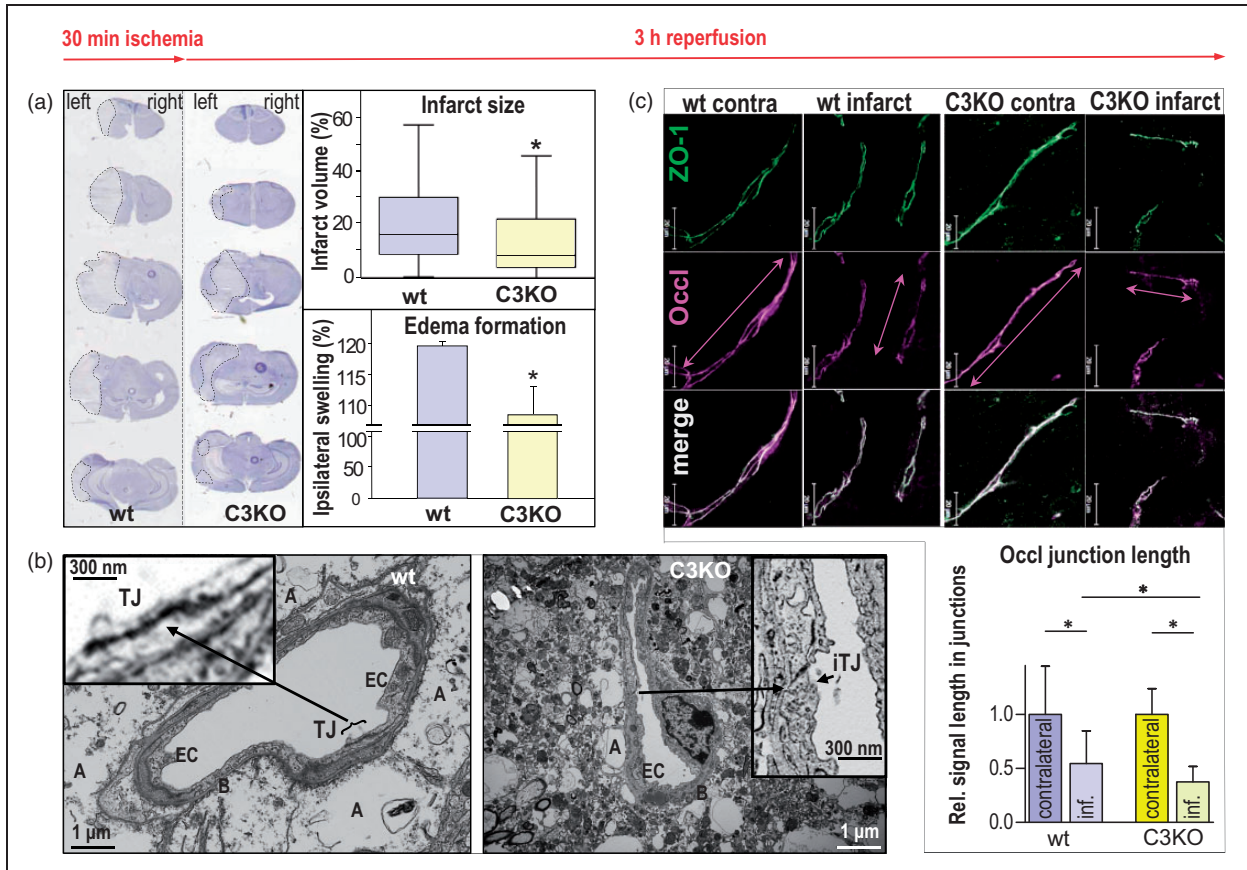


Figure 5. Forty-eight hours after 30 min transient middle cerebral artery occlusion (tMCAO), reduction in infarction, swelling, tight junction density and length of junctional occludin (Occl) is caused in brains of claudin-3 knockout mice (C3KO) compared to that from wild type (wt) brain. (a) Hematoxylin staining (left panels) showed lower infarct size (dotted lines) and ipsilateral swelling in C3KO, as confirmed quantitatively (right diagrams). Mean \pm SD, $n = 21$; $p < 0.05$; Mann–Whitney test. (b) In transmission electron microscopy of cross-sectioned brain capillaries from the striatum, the tight junctions (TJs) between endothelial cell (EC) surfaces were weakened after tMCAO in the infarct area of C3KO compared to TJs in the infarct area of wt. In wt, TJs were identified in 90% of the capillaries (left micrograph), whereas TJs were detectable in 43% of the capillaries from C3KO only. In C3KO, the junctions could hardly be identified (right micrograph) due to impairment of TJs and cell membranes. The latter is accompanied by less swollen astrocytic endfeet. A: astrocytic endfeet; B: basement membrane; iTJ: intermittent tight junction. (c) In immunohistochemistry, the length of Occl-positive segments in cell junctions (Occl junction length, measured along the vascular axis) was shorter in the C3KO infarction region than in the wt infarction area (compare double arrows); cf. lower part of (c) for quantification (inf., infarct). Zonula occludens protein 1 (ZO-1) was used as a junction marker protein. Scale bars, 20 μ m; mean \pm SD, $n = 47$ –60; $p < 0.05$; Kruskal–Wallis test with Dunn's multiple comparison.

comprehensive evidence obtained in other organs,⁷ our findings indicate that Cldn3 enhances BBB sealing and TJ complexity. The tightening effect is not only related to Cldn3: the decreased expression of Cldn3 and Cldn1 is correlated, and this may potentiate their influence on the TJs.

A typical ischemic stroke causes cytotoxic edema, and this mainly results in swelling of perivascular astrocytic endfeet.⁵ Surprisingly, infarcts are smaller and the cytotoxic edema is clearly reduced in brains of Cldn3 knockout mice, where the endothelial TJs are much slimmer and the perivascular astrocytic endfeet are less swollen than in the control. This suggests better

paraendothelial fluid drainage from astrocytes into the vasculature. In astrocytic endfeet, the water channel aquaporin-4 is strongly expressed, allowing free water exchange. This is possible, as water movement through aquaporins is a passive, osmotically driven process.⁵⁶ Finally, fluid diffuses through the BBB due to the dysfunction of the paraendothelial barrier, as similarly reported for TJs of Cldn3-free hepatocytes.⁵⁰

From a pathological point of view, our investigation demonstrates that intact TJs as in wild type endothelial cells protect the BBB, but promote edema and infarct size. Conversely, with compromised TJs as seen in C3KO mice, endothelial injury is intensified, whereas

the extent of stroke is alleviated. Taking this into account, modulation of tightening claudins expressed at the BBB would be a new strategy to combat stroke. A Cldn1-based example is the peptidomimetic C1C2, that affects paraendothelial tightness in a cell culture model of the BBB.⁵⁷ Suppression of Cldn5 is also feasible by administration of the Cldn5 peptidomimetic C5C2⁵⁸ or Cldn5-specific siRNA.⁵⁹ For some hours, C5C2 moderately increases the permeability of the mouse BBB for small molecules.⁵⁸ Following traumatic brain injury, the more protracted siRNA effect temporarily and size-selectively modulates the BBB and decreases cerebral edema.⁵⁹

These observations may have profound consequences for the treatment of postischemic stroke, where cerebral edema is a hallmark of the pathogenesis. Of course, several different aspects, such as inflammatory processes (which are beyond the scope of this study), have to be explored in further studies on the role of TJ protein expression in ischemia. Nevertheless, a transient and moderate increase in TJ permeability should still be effective at a later time point after the onset of stroke. Both peptide-based downregulation of Cldn3⁵⁷ and of Cldn5 by a peptidomimetic or siRNA were effective between 2 h⁵⁸ and 24 h.⁵⁹ This interval is consistent with the time frame we observed for perivascular swelling in the stroke area. Consequently, a “downsizing” procedure could be applicable to achieve transient detumescence of edema by suppressing endothelial claudins within a couple of hours. This would be a promising approach for a markedly later treatment of stroke, as therapy is currently restricted to the first 4.5 h.⁶⁰

In conclusion, the results provide evidence that intact TJs in the microvasculature of the brain play an ambivalent role. When the TJs appear electron dense and seal the cleft bidirectionally between the endothelial cells, they prevent paraendothelial flow, leading to larger infarctions and greater edema in the affected brain area. Conversely, an attenuated infarct process was observed if the TJ structure was less dense or less complex. These findings could be a basis for new approaches for limiting the extent of stroke.

Funding

The author(s) disclosed receipt of the following financial support for the research, authorship, and/or publication of this article: This work was supported by BMBF VIP03V0647, DFG SFB/TR23 B7, LOEWE Initiative Hessen (III L 4-518/55.004, 2009), Excellence Cluster Cardio-Pulmonary System, Frankfurt Hospital Foundation, FP7 EU Health consortium JUSTBRAIN.

Acknowledgements

The authors thank M. Dopatka (Experimental Neurology, Charite Berlin) for outstanding technical support during the MCAO studies and S. Müller (Charité Stroke Center) for expert MRI measurements. This study also benefited from excellent support for electron microscopy by M. Ringling (FMP) and R. Knittel (Univ. Tübingen).

Declaration of conflicting interests


The author(s) declared no potential conflicts of interest with respect to the research, authorship, and/or publication of this article.

Authors' contributions


Animal experimentation and/or biochemical experiments were planned and accomplished by LW, RB, OBK, PB, SD, HCH, KD, MK, ZQ, SL, AVA, AR, electron microscopy by DP and HW. LW, RFH and IEB were involved in data evaluation and drafted the manuscript.

ORCID iDs

Lars Winkler  <https://orcid.org/0000-0003-3350-1189>

Olga Breikreuz-Korff  <https://orcid.org/0000-0002-7837-039X>

Kavi Devraj  <https://orcid.org/0000-0002-5005-3413>

Reiner F Haseloff  <https://orcid.org/0000-0001-9005-5993>

Supplementary material

Supplemental material for this article is available online.

References

- Roy-O'Reilly M and McCullough LD. Age and sex are critical factors in ischemic stroke pathology. *Endocrinology* 2018; 159: 3120–3131.
- Benjamin EJ, Blaha MJ, Chiuve SE, et al. Heart disease and stroke statistics-2017 update a report from the American Heart Association. *Circulation* 2017; 135: E146–E603.
- Saunders NR, Liddelow SA and Dziegielewska KM. Barrier mechanisms in the developing brain. *Front Pharmacol* 2012; 3: 46.
- Sandoval KE and Witt KA. Blood-brain barrier tight junction permeability and ischemic stroke. *Neurobiol Dis* 2008; 32: 200–219.
- Michinaga S and Koyama Y. Pathogenesis of brain edema and investigation into anti-edema drugs. *Int J Mol Sci* 2015; 16: 9949–9975.
- Krause G, Winkler L, Mueller SL, et al. Structure and function of claudins. *Biochim Biophys Acta Biomemb* 2008; 1778: 631–645.
- Gunzel D and Yu ASL. Claudins and the modulation of tight junction permeability. *Physiol Rev* 2013; 93: 525–569.
- Haseloff RF, Dithmer S, Winkler L, et al. Transmembrane proteins of the tight junctions at the

- blood-brain barrier: structural and functional aspects. *Semin Cell Dev Biol* 2015; 38: 16–25.
9. Keep RF, Andjelkovic AV, Xiang JM, et al. Brain endothelial cell junctions after cerebral hemorrhage: changes, mechanisms and therapeutic targets. *J Cereb Blood Flow Metab* 2018; 38: 1255–1275.
 10. Fletcher NF, Wilson GK, Murray J, et al. Hepatitis C virus infects the endothelial cells of the blood-brain barrier. *Gastroenterology* 2012; 142: 634–649.
 11. Hartz AMS, Bauer B, Soldner ELB, et al. Amyloid-beta contributes to blood-brain barrier leakage in transgenic human amyloid precursor protein mice and in humans with cerebral amyloid angiopathy. *Stroke* 2012; 43: 514–523.
 12. Wolburg H, Wolburg-Buchholz K, Kraus J, et al. Localization of claudin-3 in tight junctions of the blood-brain barrier is selectively lost during experimental autoimmune encephalomyelitis and human glioblastoma multiforme. *Acta Neuropathol* 2003; 105: 586–592.
 13. Nitta T, Hata M, Gotoh S, et al. Size-selective loosening of the blood-brain barrier in claudin-5-deficient mice. *J Cell Biol* 2003; 161: 653–660.
 14. Uchida Y, Sumiya T, Tachikawa M, et al. Involvement of claudin-11 in disruption of blood-brain, -spinal cord, and -arachnoid barriers in multiple sclerosis. *Mol Neurobiol* 2019; 56: 2039–2056.
 15. Berndt P, Winkler L, Cording J, et al. Tight junction proteins at the blood-brain barrier: far more than claudin-5. *Cell Mol Life Sci* 2019; 76: 1987–2002.
 16. Kooij G, Kopplin K, Blasig R, et al. Disturbed function of the blood-cerebrospinal fluid barrier aggravates neuroinflammation. *Acta Neuropathol* 2014; 128: 267–277.
 17. Furuse M, Hata M, Furuse K, et al. Claudin-based tight junctions are crucial for the mammalian epidermal barrier: a lesson from claudin-1-deficient mice. *J Cell Biol* 2002; 156: 1099–1111.
 18. Kratzer I, Vasiljevic A, Rey C, et al. Complexity and developmental changes in the expression pattern of claudins at the blood-CSF barrier. *Histochem Cell Biol* 2012; 138: 861–879.
 19. Paganelli M, Stephenne X, Gilis A, et al. Neonatal ichthyosis and sclerosing cholangitis syndrome: extremely variable liver disease severity from claudin-1 deficiency. *J Pediatr Gastroenterol Nutr* 2011; 53: 350–354.
 20. Piontek J, Fritzsche S, Cording J, et al. Elucidating the principles of the molecular organization of heteropolymeric tight junction strands. *Cell Mol Life Sci* 2011; 68: 3903–3918.
 21. Milatz S, Krug SM, Rosenthal R, et al. Claudin-3 acts as a sealing component of the tight junction for ions of either charge and uncharged solutes. *Biochim Biophys Acta Biomemb* 2010; 1798: 2048–2057.
 22. Bauer HC, Krizbai IA, Bauer H, et al. “You Shall Not Pass”-tight junctions of the blood brain barrier. *Front Neurosci* 2014; 8: 392.
 23. Marchiando AM, Shen L, Graham WV, et al. Caveolin-1-dependent occludin endocytosis is required for TNF-induced tight junction regulation in vivo. *J Cell Biol* 2010; 189: 111–126.
 24. Bellmann C, Schreivogel S, Gunther R, et al. Highly conserved cysteines are involved in the oligomerization of occludin-redox dependency of the second extracellular loop. *Antioxid Redox Signal* 2014; 20: 855–867.
 25. Cording J, Gunther R, Vigolo E, et al. Redox regulation of cell contacts by tricellulin and occludin: redox-sensitive cysteine sites in tricellulin regulate both tri- and bicellular junctions in tissue barriers as shown in hypoxia and ischemia. *Antioxid Redox Signal* 2015; 23: 1035–1049.
 26. Castro V, Bertrand L, Luethen M, et al. Occludin controls HIV transcription in brain pericytes via regulation of SIRT-1 activation. *FASEB J* 2016; 30: 1234–1246.
 27. Cording J, Berg J, Kading N, et al. In tight junctions, claudins regulate the interactions between occludin, tricellulin and marvelD3, which, inversely, modulate claudin oligomerization. *J Cell Sci* 2013; 126: 554–564.
 28. Liu PT, Jenkins NA and Copeland NG. A highly efficient recombineering-based method for generating conditional knockout mutations. *Genome Res* 2003; 13: 476–484.
 29. Willnow TE and Herz J. Homologous recombination for gene replacement in mouse-cell lines. In: Roth MG (ed) *Methods in cell biology*, vol. 43: protein expression in animal cells. San Diego, USA: Elsevier Science Publishing Co Inc, 1994, pp.305–334.
 30. Stober F, Baldauf K, Ziabreva I, et al. Single-cell resolution mapping of neuronal damage in acute focal cerebral ischemia using thallium autometallography. *J Cereb Blood Flow Metab* 2014; 34: 144–152.
 31. Endres M, Wang ZQ, Namura S, et al. Ischemic brain injury is mediated by the activation of poly(ADP-ribose) polymerase. *J Cereb Blood Flow Metab* 1997; 17: 1143–1151.
 32. Balkaya M, Krober JM, Rex A, et al. Assessing post-stroke behavior in mouse models of focal ischemia. *J Cereb Blood Flow Metab* 2013; 33: 330–338.
 33. Donath S, An JF, Lee SLL, et al. Interaction of ARC and daxx: a novel endogenous target to preserve motor function and cell loss after focal brain ischemia in mice. *J Neurosci* 2016; 36: 8132–8148.
 34. Leithner C, Fuchtemeier M, Jorks D, et al. Infarct volume prediction by early magnetic resonance imaging in a murine stroke model depends on ischemia duration and time of imaging. *Stroke* 2015; 46: 3249–3259.
 35. Hoffmann CJ, Harms U, Rex A, et al. Vascular signal transducer and activator of transcription-3 promotes angiogenesis and neuroplasticity long-term after stroke. *Circulation* 2015; 131: 1772–1782.
 36. Del Vecchio G, Tscheik C, Tenz K, et al. Sodium caprate transiently opens claudin-5-containing barriers at tight junctions of epithelial and endothelial cells. *Mol Pharm* 2012; 9: 2523–2533.
 37. Haseloff RF, Krause E, Bigl M, et al. Differential protein expression in brain capillary endothelial cells induced by hypoxia and posthypoxic reoxygenation. *Proteomics* 2006; 6: 1803–1809.
 38. Gurnik S, Devraj K, Macas J, et al. Angiopoietin-2-induced blood-brain barrier compromise and increased

- stroke size are rescued by VE-PTP-dependent restoration of Tie2 signaling. *Acta Neuropathol* 2016; 131: 753–773.
39. Tilling T, Korte D, Hoheisel D, et al. Basement membrane proteins influence brain capillary endothelial barrier function in vitro. *J Neurochem* 1998; 71: 1151–1157.
 40. Czupalla CJ, Liebner S and Devraj K. In vitro models of the blood-brain barrier. *Methods Mol Biol* 2014; 1135: 415–437.
 41. Wolburg H, Liebner S and Lippoldt A. Freeze-fracture studies of cerebral endothelial tight junctions. *Methods Mol Med* 2003; 89: 51–66.
 42. Kaya M and Ahishali B. Assessment of permeability in barrier type of endothelium in brain using tracers: Evans blue, sodium fluorescein, and horseradish peroxidase. *Methods Mol Biol* 2011; 763: 369–382.
 43. Kaufmann R, Piontek J, Grull F, et al. Visualization and quantitative analysis of reconstituted tight junctions using localization microscopy. *PLoS One* 2012; 7: e31128.
 44. Jiang XY, Andjelkovic AV, Zhu L, et al. Blood-brain barrier dysfunction and recovery after ischemic stroke. *Prog Neurobiol* 2018; 163: 144–171.
 45. Weuste M, Wurm A, Iandiev I, et al. HB-EGF: increase in the ischemic rat retina and inhibition of osmotic glial cell swelling. *Biochem Biophys Res Commun* 2006; 347: 310–318.
 46. McCaffrey G, Willis CL, Staatz WD, et al. Occludin oligomeric assemblies at tight junctions of the blood-brain barrier are altered by hypoxia and reoxygenation stress. *J Neurochem* 2009; 110: 58–71.
 47. Jiao HX, Wang ZH, Liu YH, et al. Specific role of tight junction proteins claudin-5, occludin, and ZO-1 of the blood-brain barrier in a focal cerebral ischemic insult. *J Mol Neurosci* 2011; 44: 130–139.
 48. Saitou M, Furuse M, Sasaki H, et al. Complex phenotype of mice lacking occludin, a component of tight junction strands. *Mol Biol Cell* 2000; 11: 4131–4142.
 49. Castro Dias M, Coisne C, Lazarevic I, et al. Claudin-3-deficient C57BL/6J mice display intact brain barriers. *Sci Rep* 2019; 9: 203.
 50. Tanaka H, Imasato M, Yamazaki Y, et al. Claudin-3 regulates bile canalicular paracellular barrier and cholesterol gallstone core formation in mice. *J Hepatol* 2018; 69: 1308–1316.
 51. Wilhelm I, Nyul-Toth A, Suciú M, et al. Heterogeneity of the blood-brain barrier. *Tissue Barriers* 2016; 4: e1143544.
 52. Xu HM, Hu F, Sado Y, et al. Maturation changes in laminin, fibronectin, collagen IV, and perlecan in germinal matrix, cortex, and white matter and effect of beta-methasone. *J Neurosci Res* 2008; 86: 1482–1500.
 53. Coomber BL and Stewart PA. Morphometric analysis of CNS microvascular endothelium. *Microvasc Res* 1985; 30: 99–115.
 54. Petrov T, Howarth AG, Krukoff TL, et al. Distribution of the tight junction-associated protein ZO-1 in circumventricular organs of the CNS. *Mol Brain Res* 1994; 21: 235–246.
 55. Benz F, Wichitnaowarat V, Lehmann M, et al. Low wnt/beta-catenin signaling determines leaky vessels in the subfornical organ and affects water homeostasis in mice. *Elife* 2019; 8: e43818.
 56. Hsu Y, Tran M and Linninger AA. Dynamic regulation of aquaporin-4 water channels in neurological disorders. *Croat Med J* 2015; 56: 401–421.
 57. Staat C, Coisne C, Dabrowski S, et al. Mode of action of claudin peptidomimetics in the transient opening of cellular tight junction barriers. *Biomaterials* 2015; 54: 9–20.
 58. Dithmer S, Staat C, Muller C, et al. Claudin peptidomimetics modulate tissue barriers for enhanced drug delivery. *Ann NY Acad Sci* 2017; 1397: 169–184.
 59. Campbell M, Hanrahan F, Gobbo OL, et al. Targeted suppression of claudin-5 decreases cerebral oedema and improves cognitive outcome following traumatic brain injury. *Nat Commun* 2012; 3: 849.
 60. Peplow PV. Neuroimmunomodulatory effects of transcranial laser therapy combined with intravenous tPA administration for acute cerebral ischemic injury. *Neural Regen Res* 2015; 10: 1186–1190.
 61. Gonzalez-Mariscal L, Quiros M and Diaz-Coranguez M. ZO proteins and redox-dependent processes. *Antioxid Redox Signal* 2011; 15: 1235–1253.